PCCP

Accepted Manuscript

ROYAL SOCIETY OF CHEMISTRY

www.rsc.org/pccp

The effect of substituted 1,2,4-triazole moiety on the emission, phosphorescent properties of the blue emitting hetroleptic iridium (III) complexes and the OLED performance: a theoretical study

Ruby Srivastava*, Laxmikanth Rao Joshi

Inorganic & Physical Chemistry Division, CSIR-Indian Institute of Chemical Technology
Hyderabad-500607, India

Abstract:

A series of neutral heteroleptic mononuclear iridium (III) complexes were investigated by using density functional theory /time-dependent density functional theory (DFT/TD-DFT) approach to determine the effect of substituted 1,2,4-triazole moiety on the electronic structures, emission, phosphorescent properties and the OLED performance. The result reveals that substituting of the free position in triazole ring by the $–PhOCH_3$(**2**) which provides the higher emission energy and lower oscillator strength, leads to larger radiative lifetime values mainly due to the LLCT transition character. The evaluation based on one- center spin-orbit coupling produces the higher k_r values for the substituent $–F_5Ph$ (**5**) with smaller ΔE(S-T) value. Furthermore, we also investigated the performance of the OLED device, which includes the charge injection/transport/balance ability, increases the Förster energy transfer rate and triplet exciton confinement for host and guest materials of blue emitting Ir (III) complexes. Finally, we hope that our investigations would help the design of high efficient phosphorescent materials.

Keywords: DFT, TDDFT, SOC, MLCT, iridium complexes

Address for correspondence:

*Corresponding author:

E-mail address: amitruby1@gmail.com (Ruby Srivastava); Phone: +91-040-27191430.

1. Introduction

The synthesis and photophysics of Ir (III) complexes has witnessed great interest as these complexes represent the most effective, tunable and sublimable phosphorescent materials for organic light emitting diode (OLEDs) fabrication.[1,2] OLEDs are also utilized by the experts in other photonic applications as sensors, probes, imaging agents and photosensitizers of electron and energy transfer.[3] The strong spin-orbit coupling caused by heavy metal organometallic ions in these complexes facilitates the intersystem crossing from the singlet to triplet state in which the statistical ratio is 1:3.[4-6] As a substantial involvement of metal *d* orbitals in the bonding relaxes selection rules for spin forbidden transitions, emission from higher multiplicities are observed.[7] Since the remainder 75% of triplet states can also be emissive, 100% internal quantum efficiency (IQE) in principle, can be obtained. Red[8] and green[9] emitting Ir (III) complexes have been successfully fabricated from years with high quantum efficiencies, achieving blue phosphorescence with high quantum efficiency is still a challenge.[10-12] So, several strategies have been developed to shift the emission to blue colour. This can be obtained by increasing the contribution from the metal to ligand chage transfer (^{3}MLCT) in the lowest-lying triplet manifold or a mixed state with MLCT and ligand-centered (LC) for high-energy emitting species.[13-15]

The emission color shifts to blue either on adding the electron withdrawing group (fluorine) with 2,4 difluorophenyl pyridyl (dfppy) cyclometalated ligand for FIrpic, FIr6, FIrtaz [8,11,14-15] and others [16] in which the electron-withdrawing groups stabilizes the HOMO and thus increases the HOMO–LUMO gap [17-18] or by changing the ancillary ligands coordinated to Ir (III) from aromatic groups to cyano [10,19] and isocyanide[20] derivatives. Though using the σ-donating ligands (as carbene) is the extremely successful approach in obtaining the *true blue* light even in near UV region. It has been reported that *fac* Ir(CNpmb)$_3$ has obtained the higher quantum yield (0.78) for the substituted tris (phenylbenzimidazolinato) iridium carbene complexes as a blue phosphorescent material. [21] In general, prediction and design of the properties of these luminescent complexes are related to the σ-donating and electron accepting capabilities of the coordinating ligands.[11] Therefore to get a better insight of the effects of substituents**,** we have selected five

heteroleptic Ir (III) complexes with two 4,6-diflourophenylpyridine ligands and third 1,2,4-triazol-3-yl pyridine ancillary ligand with different substituents in the 5 position. The formula for the complexes is $\{(F_2ppy)_2Ir(pta\text{-}X)\}$ where X-Me (**1**), PhOMe (**2**), 4FPh (**3**), 3,5FPh (**4**) and F_5Ph (**5**) synthesized by Borner et al.[22] Azole ligands are strong sigma donor and weak π acceptor ligand due to the electron–rich nature of the five-membered aromatic rings.[23] 1, 2, 4-triazoles are of interest due to the azole ring upon co-ordination forms anionic nitrogen, which leads to a neutral complex. We have attempted to systematically study the structural, opto-electronic, photo physical properties and the better OLED performance in detail. First principle theoretical analysis is sometimes reliable in analyzing the electronic structures and the excited state transitions of transition metal complexes as there is always significant level of uncertainty in all DFT and TDDFT calculations, which heavily depends on the functional approximations used in the method.[24-27]

The discussion is organized as follows: Initially the geometrical stability of the electronic structures of these five complexes, the nature- type as well as the percentage molecular orbital contributions from the different ligands, absorption spectra in solvent and the evaluation of excited state lifetimes τ (μs) are discussed. Later on the discussion is shifted to the evaluation of spin –orbital coupling (SOC) matrix element and prediction of radiative rate constant k_r (s^{-1}) and lastly the phosphorescent properties and the better performance as OLED is discussed, which includes the charge injection/transport and balance ability, discussing the energy transfer rate and triplet exciton confinement for host and guest materials, followed by the conclusions.

2. Computational details

Calculations on electronic singlet and triplet states of all studied complexes were carried out by using density functional theory (DFT)[28] with the hybrid-type Perdew–Burke–Ernzerhof exchange correlation functional (PBE0) and the unrestricted PBE0 (UPBE0), respectively.[29] There were no symmetry constraints on these complexes. Vibrational frequencies were calculated at the same theoretical level to confirm that each

configuration was a minimum on the potential energy surface. On the basis of the optimized structures of the ground and excited states, the absorption and emission properties in dichloromethane (CH_2Cl_2) medium were calculated by time-dependent density functional theory (TD DFT)[30] associated with the polarized continuum model (PCM).[31,32] In all calculations, a "double-ξ" quality basis set LANL2DZ[33] associated with the pseudopotential was employed on the iridium atom, in which a relativistic effective core potential (ECP) on Ir replaces the inner core electrons, leaving the outer core $5s^2 5p^6$ and $5d^6$ as the valence electrons of Ir (III). The 6- 31G* basis set was used for non-metal atoms in the gradient optimizations. In addition, the properties of the iridium (III) complexes, such as the ionization potential (IP), electron affinity (EA), hole extraction potential (HEP), electron extraction potential (EEP), reorganization energy (λ) and HOMO–LUMO gap (Δ_{H-L}) were also obtained at the same PBE0/LANL2DZ level. For all calculations the Gaussian 09 software package of programs [34] was used. GaussSum 2.5 [35] was used for orbital and the DOS analysis as well as UV/Vis spectra analysis and Gauss View interface[34] for structures and orbital manipulations. NBO [36] analysis has been carried out to obtained the coefficients of natural atomic orbitals for the evaluation of spin-orbital coupling (SOC) and to obtained the stabilization energy *E(2)* for all possible interactions of these substituents between "filled" (donor) Lewis-type NBOs and "empty" (acceptor) non-Lewis NBOs and estimating their energetic importance by second-order perturbation theory. Further, the methodology for calculating the radiative lifetimes, reorganization energies and the energy transfer rate between the guest / host materials and the evaluation of radiative rate constant are discussed in the following sections.

2.1 Radiative lifetime

The radiative lifetimes (τ) for spontaneous emission were investigated by using the Einstein transition probabilities. The oscillator strength and fluorescence lifetime associated with every spin sublevel of the single emission state (S_1^k) are described by (in atomic units):[37]

$$\frac{1}{\tau_k} = \frac{4\,\omega_1^3 \alpha^3}{3} \sum_l \left| \langle\, ^1 0 | r_l |^3 S_1^k \rangle \right|^2 \qquad (1)$$

$$f_k = \frac{2\omega_1}{3} \sum_l \left| \langle\, ^1 0 | r_l |^3 S_1^k \rangle \right|^2 \qquad (2)$$

where ω_1 is the transition energy(emission) , $\boldsymbol{\alpha}$ is the fine structure constant, $\boldsymbol{\alpha} \approx 1/137$ and r_l are the *x, y,* z-th components of the electric dipole operator.

2.2. Reorganization energy

According to Marcus/Hush model,[38,39] the rate of intermolecular charge transfer (k_{ET}) can be estimated by using the semi-classical Marcus theory as follows :

$$k_{ET} = \frac{4\pi^2}{h} \frac{1}{\sqrt{4\pi\lambda k_B T}}\ \beta^2 \exp\left(-\frac{\lambda}{4k_B T}\right) \qquad (3)$$

Where β is the transfer integral between the neighboring molecules, T is the temperature, h and k_B are Planck and Boltzmann constant respectively and λ is the reorganization which plays a key role in charge transfer rate for OLEDs.[40] Hence, the reorganization energy for hole transfer in Eqn (2) can be defined as

$$\lambda_{hole} = \lambda_+ + \lambda_0 = [E^+(M) - E^+(M^+)] + [E(M^+)] + [E(M^+) - E(M)]$$

$$= [E^+(M) - E(M)] - [E^+(M^+) - E(M^+)] \qquad (4)$$

Thus, the reorganization energy for hole (λ_h) and electron transport (λ_e) can be evaluated as [41]:

$$\lambda_h = IP_V - HEP \qquad (5)$$

$$\lambda_e = EEP - EA_V \qquad (6)$$

E (M) and $E^+(M^+)$ represent the energies of the neutral and cation species in their lowest energy geometries respectively, while *E* (M^+) and $E^+(M)$ represent the energies of the cation and neutral species respectively. Conjugation length, substituents and heteroatom identity are also some factors, which dictates λ, but this description holds only for harmonic potential energy surfaces and when the λ_+ and λ_0 energy values are close.

2.3. Energy transfer rate

Basically the energy transfer rate between the guest and the host materials (in theory) can be evaluated by [42] as

$$W_{i\rightarrow j} = \frac{2\pi}{h}\left|\langle\Psi_i|V|\Psi_j\rangle\right|^2.FC \qquad (7)$$

Where $W_{i\rightarrow j}$ represents the energy transfer rate from the initial state *i* to the final state *j*, *FC* denotes the Frank-Condon factor.

For Förster energy transfer, $\left|\langle\Psi_i|V|\Psi_j\rangle\right|^2$ can be given as:

$$\left|\langle\Psi_i|V|\Psi_j\rangle\right|^2 = \kappa^2 \left|\frac{\mu_D\mu_A}{4\pi\varepsilon_0\varepsilon_r R_{DA}^3}\right|^2 \qquad (8)$$

2.4. Radiative decay rate

The admixture of emissive singlet states into the lowest triplet state, due to the effect of iridium, gives rise to the phosphorescence of transition metal complexes. Theoretically, radiative rate constant (k_r) is related to the mixing between S_1 and T_1, as expressed below:

$$K_r(T_1) \approx \frac{n^3 {E_T}^3}{1.5}\left(\frac{\langle S|H_{SO}|T\rangle}{E_S - E_T}\right)^2 \times \frac{f_s}{E_s} \qquad (9)$$

where E_S, E_T are in (eV) and matrix element are in cm^{-1}. n is the refractive index of the medium and f_s is the oscillator strength (singlet state) . Among the spin-orbit coupling at the triplet sublevels of T_1($d_{xy} \rightarrow \pi^*$), that is , $T_{1,x}$, $T_{1,y}$, and $T_{1,z}$, only the element involving $T_{1,y}$ has a non-zero value. Accordingly, only considering the element between spin orbitals involving ζ $(=d_{xy})$ and $\zeta(=d_{yz})$ indicated by eq.(9) in ref.[45] or eq.(67) in ref.[46], the one-center spin-orbit coupling SOC element can be simply evaluated as :

$$\langle S_2 | H_{SO} | T_{1,y} \rangle = \frac{1}{2}(\langle C_{dxy}\, d^{\alpha}{}_{xy} \mid H_{SO} \mid C_{dyz} d^{\beta}{}_{yz} \rangle - \langle C_{dxy} d^{\beta}{}_{xy} \mid H_{SO} \mid C_{dyz} d^{\alpha}{}_{yz} \rangle)$$

$$= \frac{1}{2} \zeta_{Ir-5d} C_{dxy} C_{dyz} \qquad \textbf{(10)}$$

With respect to the eq. (10), $\zeta_{Ir\text{-}5d}$ represents the one electron SOC constant of the *5d* electron of Ir ion and C_{dxy} and C_{dxz} represents the coefficients of the *5d* orbital related to HOMO and HOMO-1 respectively. Furthermore, theoretical values of $\zeta_{Ir\text{-}5d}$ = 4430 cm^{-1} for the Ir (III) ion [47,48] is also used in the present article. We could thus evaluate the SOC value by deducing the parameters in eq. (10) through the calculations of TD DFT method. Thus we assess the phosphorescence mechanism by calculating the k_r value using a crude approximation of the model of the aforesaid one-center SOC element, together with the eqs. (9) and (10).

3. Results and Discussion

3.1 Ground state structural properties

The sketch drawing of the five molecules are represented in Figure 1. The main geometry structural parameters together with the experimental X-ray crystal data is given in Supplementary Table-1. It is well known that the observed differences in opto-electronic and photophysical properties of these complexes depend mainly on the ground

state electronic structure. So to get a better understanding of these molecular structures, the optimized geometry parameters for the ground states and triplet states of investigated molecules are tabulated in Table 1. As shown in Figure 1, all complexes show a pseudo octahedral co-ordination around the central iridium atom. The di-flouro phenylpyridine (F_2ppy) ligands have Ir-N bond-length between 2.023-2.042 Å and Ir-C between 2.00-2.02 Å[15, 49]which are in very good agreement with the calculated results as the Ir-C have 1.99-2.01 Å. Ir-N of **1** and **2** are not effected much by adding -Me and -OMe electron-donating substituent to the triazole, but slightly increased more in **3, 4** and **5** while adding the electron withdrawing groups -4FPh, -3,5FPh and $-F_5$Ph substituents. This can be rationalized as the π-accepting ability of triazole ring is greater than that of the pyridine ring and can be seen by the Mulliken charges of the individual atoms given in Supplementary Table 2. The slight difference of the calculated metal-ligand distances can be attributed to the crystal packing in crystalline state.

The bond-angles N3-Ir-N4 have a small 0.2^0 difference between the experimental and the theoretical values. The C-Ir-N has a mean difference of $0.2\text{-}0.5^0$ with the experimental values. The Ir-N bond for **1** and **2** are more in T_1 states for **1-4** complexes while for complex **5**, the bond is contracted compared with those in S_0 states. If the bond-length of Ir-C1 is slightly larger, then it shows a contracted Ir-C2 in 1-**5**. Similar trend is observed in Ir-N3 and Ir-N4 bonds. Because of the stronger interaction between metal and F_2ppy in **3-5,** F_2ppy ligand will have a greater effect on the frontier molecular orbitals (FMOs) in both the ground state and the excited state. Furthermore, this different strength between the metal and the F_2ppy and electron donating –Me (**1**), -PhOMe (**2**) and electron withdrawing -4FPh (**3**), -3,5FPh (**4**) and -F_5Ph (**5**) will result in different electron transition characters.

3.2 Molecular orbital properties in the ground state

Since the frontier molecular orbital (FMO) is key to get a better understanding of optical and chemical properties of these complexes, we have aimed this section to implement the detailed examination on pertinent orbitals. The electron density

distributions and FMO energy levels of **1**-**5** with the FMO levels for host are given in Figure 2. In theory, the HOMO-LUMO gap of molecule is the orbital energy difference between the HOMO and LUMO, termed as HOMO-LUMO gap (Δ_{H-L}). The optical band gap (E_g) is actually the energy difference between the S_0 and S_1 state, not the orbital energy difference between the HOMO and LUMO. Experimentally optical band gap (E_g) obtained from the spectra is the lowest transition or excitation energy from the ground state to the first dipole allowed excited state, considering only an electron, which is promoted from the HOMO to the LUMO. It has been assumed that the lowest singlet excited state can be described by only one singly excited configuration. The Δ_{H-L} (eV) and E_g both have values in the decreasing order as **5**>**4**>**3**>**1**>**2**. The Δ_{H-L} gap is highest for **5 (**4.00 eV) and lowest for **2** (3.57 eV) in the studied complexes. (Supplementary Table-3).

Furthermore, numeric percentage orbital contribution of metal and ligands are collected in Supplementary Table 4. For complex **1,** HOMO mainly resides on the pta moiety and the composition of dπ is only 11.8 %. The HOMO of **2** is also having the similar distribution to **1**. The HOMOs of **1** & **2** have energy values 5.73 eV and 5.18 eV, which are almost isolated orbital. The attached electron donating group $–CH_3$ and $–PhOCH_3$ pull the electron density towards the ending substituent with the proportion on the ancillary ligand increased to 28.2% and 91.9%. HOMO-1 contributes to 65.2% by the (F2ppy) and HOMO-2 shows the 72.3% contribution by the (pta) group. The LUMO for **1** and **2** lie above the HOMOs with contribution of 78.8% and 82% from F_2ppy ligands. The LUMO+1 have $\pi^*(F_2ppy)$ 74.6% for complex **1** and π^*(pta) 63% for complex **2**. The lowest excited state involves the F_2ppy ligands even though for fluorine derivative due to the torsion angle between the triazole and the fluorinated phenyl ring.[22] In complex **3, 4, 5** the trend is consistent as the contribution of ancillary group in HOMO is 71.7%, 87.4% and 80.7% respectively. The LUMO for these complexes have the contribution of 84.7% $\pi^*(F_2ppy)$, 63.5% $\pi^*(F_2ppy)$ and 59.5% $\pi^*(F_2ppy)$ respectively. The LUMO+1 has ancillary ligand contribution of 87.1% (4FPh), 79.8% (3,5FPh) and 61.5% (F_5Ph) respectively. LUMO+2 have contribution from (F_2ppy) of 89.4%, 84.8% and 92% respectively. The other transition from HOMO-5 to LUMO+5 are also listed in

Supplementary Table 4. Though giving too much meaning to the molecular orbitals by DFT might be misleading, yet the ordering of HOMOs and LUMOs provide a reasonable qualitative indication of the excitation energies. [50]

The energy levels of HOMO and LUMO are greatly influenced by the electron-donating and electron with-drawing substituents on the ancillary ligands. Among **1-3**, electron-donating group -OCH_3 (**2**) can destabilize both of the HOMO and LUMO energy levels while electron–withdrawing group, -F (**3**) stabilizes the HOMO energy and destabilizes the LUMO level, which results in the largest H-L gap of 3.85 eV among the first three complexes. In **4** and **5**, the substituents can stabilize both HOMO and LUMO energies to a larger extent compared to **1-3**, having energy gap of 3.90 eV and 4.00 eV respectively. In **1-3**, the raised HOMO energy levels will benefit the hole injection, while the slightly increased LUMO levels will decrease the electron injection ability and **4** and **5** have the opposite trend. The spectroscopic data for **5** with highest oxidation and lowest reduction potential agrees well with the calculated HOMO and LUMO show it to be the bluest emitter among the studied complexes. Here it should be mentioned that a direct conclusion drawn from comparison of the measured quantities of electrochemical data to the corresponding calculated HOMO-LUMO values is not a straightforward approach, as the electrochemical data refers to the adiabatic processes while the calculated values are the approximated vertical oxidation /reduction potentials.

3.3 Absorption in dichloromethane

The calculated absorption spectra associated with their oscillator strengths, assignment, configurations, excitation energies and configuration interaction (CI) coefficients, experimental wavelengths (for comparison) and the calculated triplet energies of the studied complexes are listed in Table 2. As we are going to discuss the photo physical properties in the next section, so first ten leading excited states (with CI coefficients) and first triplet energy is presented herein. The fitted Gaussian type absorption curve is depicted in Figure 3. It is observed that the experimental absorption spectra shows intense feature below 340 nm and less intense features above 340-450 nm.

These intense absorptions are assigned to π-π^* transitions which are localized on the coordinated ligands. Basically these are due to the transitions which centers at F_2ppy ligands and the shoulder of ~ 290 nm is due to the transitions at triazole ligand. For (340-450 nm), the transitions are (^{1}MLCT) metal to ligand charge transfer singlet-to-singlet and spin forbidden singlet to triplet ^{3}MLCT transitions which is the basic feature of Ir complexes in which the SOC is strong. The calculated absorption spectra can reproduce well the experimental features in terms of band positions, intensities and separations.

The intense transitions for **1** lies at 294, 334 nm having configurations of H-1→L+3 (41%) and H-1→L+1(56%) having 282 and 343 nm experimental results. For **3,** the intense transitions lies at 318 and 342 nm with 315 and 342 nm experimental values while the state configurations are H→L+3 (93%) and H-1→L+1 (76%). For **4**, the intense absorptions are observed at 307 and 343 nm with 315 and 346 nm experimental values. The assigned configurations are H→L+3 (81%) and H-1→L+1(72%) respectively. For **2** and **5**, it has been observed that the less intense transitions are observed at 358 and 341 nm with 354 and 350 nm experimental values. The configurations assigned with these values are H-1→L (87%) and H-1→L (82%) respectively. Above 340-450 nm, the less intense absorption occurs at 363(**1**), 367 (**2**), 375 (**3**), 363 (**4**) and 377 (**5**) with 374 (**1**) and 370 (**2, 3, 4, 5**) experimental values. The assigned configurations are H→L (83%), H→L (88%), H→L (76%), H-1→L (46%) and H→L (83%) respectively. The lower energy transitions are assigned to MLCT/LLCT transitions while the rest of the other transitions are assigned to MLCT/LLCT with certain amount of ILCT transitions. On one hand, this kind of transition is dipole allowed and on the other hand, the singlet- triplet transitions probably occur due to the participation of iridium. Both these two properties can ensure the high luminescence efficiency of complexes as they are strongly related to the σ-donating and electron accepting capacities of the coordinating ligands.[15]The observed strongest absorption located at the highest energy regions are 4.80, 4.75, 4.83, 4.75 and 4.83 eV [23] which agrees well with calculated values 4.68, 4.63, 4.71, 4.66 and 4.77 eV respectively in terms of trends and they are again blue shifted in the order as **5**<**3**<**1**<**4**<**2**.

3.4 Emission spectra

On the basis of optimized structures in excited state we have investigated the emission spectra of the considered molecules. The computed emission energies are all consistent with the experimental observation. [refer sec 2.1]. The $S_1 \rightarrow S_0$ flourescence peaks in emission spectra have the largest oscillator strengths in all molecules and exclusively comes from HOMO→LUMO $\pi\pi^*$ excitation. The tabulated τ values are given in the Table 3. The calculated wavelengths for (lowest energy emission) of the five complexes are localized at 428, 517, 450, 423 and 425 nm respectively which are deviated from the experimental values by 33, 25, 9, 9 and 33 nm, which is comparable to the other investigation .[51,52] The Stokes shift are 65, 144, 75, 60 and 48 nm respectively. Complex **1, 3, 4** and **5** are having shift of 48-75 nm, while **2** is having the larger shift for –PhOMe (**2**) group. The value of τ is largest for **2** as it can be justified by the synthesis results that the strong electron-donating methoxy group on the triazole, a ligand-to-ligand charge transfer (LLCT) is responsible for the longest lifetime which can be seen from Table 2. The calculated lifetime for the rest of complexes is less than the experimental lifetime values. This can be explained by the torsional angle between the triazole and the substituted phenyl ring. The larger the torsional angle, the lower the quantum yield and the excited lifetime of the complexes[22]. Though a recent study [53] on iridium (III) phenyl-triazole complexes analysed the decrease in quantum yield is correlated with a blue shift in the emission energy and suggested that thermally activated, vibrational (non radiative decay) could be responsible for the quenching of the photoluminescence. It is observed in this study that the decrease in calculated values of emission energy is mostly related to the distortion from coplanarity between the triazole and substituted phenyl ring connected to it rather than an increase in electron with-drawing properties which is also supported by the experimental results.[22]

3.5 Transport properties

A good performance of OLED device is attributed to the good charge mobilities and comparable balance between the hole and electron transport. The charge injection properties can be evaluated by the ionization potential (IPs) and electron affinity (EAs)

which are closely related to the HOMO and LUMO respectively. These IPs and EAs are used to evaluate the injection of both holes and electron and the charge transport rate and balance is estimated by reorganization energy λ. The calculated IP (IP_v), EA (EA_v) both vertical (v; at the geometry of the neutral molecule) and IP (IP_a), EA (EA_a) (a;optimized structure for both the neutral and charged molecules) and reorganization energy (λ) as well as the hole and electron extraction potentials (HEP, EEP) obtained by DFT are listed in Table-4. Here the HEP and EEP are the expressions of IP and EA respectively. HEP is the energy difference from M^+(cationic) to M (neutral molecule), using M^+ geometric structure in the calculation and EEP is the energy difference from M^-(anionic) to M, using M^- geometric structure in calculation. The two key parameters that dominate the charge-transfer rate are λ and V. λ is the reorganization energy and V is the electronic coupling matrix element, which is largely influenced by orbital overlap. [refer sec 2.2]
For photoluminescent materials, the lower IP of the emitter, the easier the entrance of holes from the hole-transport layer (HTL) to the emitter, and the higher the EA of the emitter, the easier the entrance of electrons from the electron-transport layer (ETL). For IP and EA values, we did not include the solvent polarization of the surrounding medium. SPE is used to estimate the self-trapping energies of charge in the materials, which is the energy due to the structural relaxation. In Table 4, the calculated IP (adiabatic and vertical) values increases in the following order **2<1<3<4<5**. This indicates that the difficulties of hole injection from HTL to these complexes gradually increase and it can be seen by the HOMO energy level trend also. By analysis of EA values **3**, **4** and **5** more easily accept electron than **1** and **2** which is also seen from the LUMO energy level trend.

As emitting layer materials, hole and electron injection balance is necessary. In Table 4, the reorganization energy for hole transport are more than the electron transport, which shows that electron transporting performances of these complexes are better than the hole transporting performances. Since the difference between the λ_h and λ_e of these complexes are smaller compared to other transition metal complexes, [54] therefore they are suitable as emitters in OLEDs. Results predict that the hole injection barrier from HTL to emitter are smaller for **2**, larger for **1, 3, 4** and largest for **5**, while the electron injection abilities of **1** and **2** are less and **3-5** are almost equivalent. A more stable potential well for hole trapping can be provided by higher HOMO values. So we can predict that due to the

improved ease of electron trapping and hole injection abilities, **1** and **2** should have higher EL efficiency. The SPE (h) is (~0.07-0.18 eV) and SPE (e) is (~0.07-0.09 eV) for all the reported complexes.

3.6 Comparison of performance in OLEDs

As stated above, investigation on the guest-host relationship is an important subject of research to improve the efficiency of the OLEDs. A relatively long-time of phosphorescent metal complexes can cause a long range of exciton diffusion and may lead to dominant triplet-triplet annihilation, getting quenched in the adjacent layers of materials in OLEDs. Therefore, iridium phosphors have to be widely spread into the host matrix. Excitons confinement on the guest may mainly comes from direct charge trapping as well as Förster and Dexter energy transfer from the host materials. To achieve efficient electrophosphorescence, effective host material is of prime importance. As the charge trapping and energy transfer are correlated with the FMO energy levels of different layers in the OLED device, so it is useful to investigate those related FMO levels to explore the origin of excitons and charge confined to the guest. To achieve efficient electrophosphorescence, several requirements for the effective host material have to be considered. The HOMOs and the LUMOs of the host material should match with those of neighboring active layers to lower the device driving voltage and reduce the hole and electron injection barrier. Host should possess the high triplet energies than those of the dopant emitters to confine the triplet excitons in the emissive layer and to prevent the reverse energy transfer from the guest back to the host.[55] The charge carrier transport properties for the host are expected to be good and balance for the hole electron recombination process. (As discussed in 3.5)

We have taken **TCTA** and **TPBI** host materials to compare the efficiency of our studied complexes.[22] **TCTA** is a typical hole transport (HT) host material and **TPBI** is mostly used as electron transport (ET) type host in a mixed host system or double emissive layer [48]. The comparative HOMO and LUMO energies of the host materials and the guest materials (**1-5**) are given in figure 2. It could be found that the LUMO energy

levels of five complexes have higher energy levels than the host **TCTA**, **TPBI** whose LUMO energy level is 2.40 and 2.07 eV respectively. Thus, it may be possible that guest obtains the energy through energy transfers from host to the guest. As for HOMO energy level, the HOMO values of **2** is higher and **3**,**4**,**5** are lower than **1**, suggesting that the hole injection barrier for **2** from the hole transport material directly to the guest is smaller , which may be favorable for the hole trapping. Moreover, the HOMO energy level of **2** (-5.28 eV) is higher, having better performance in hole trapping. The complexes with fluorine substituent are having lower energy than **1** and **2**, so these complexes might be good for electron trapping. Finally we can say that the complexes without fluorine substituent (**1**, **2**) could improve the hole trapping ability and the complexes (**3**,**4**,**5**) with fluorine substituent perform well in electron trapping.

Dexter energy transfer plays a significant role in obtaining the triplet excitons for the guest materials and the corresponding rate is correlated with the changes in Gibbs free energy (ΔG^0) based on Marcus electron-transfer theory. ΔG^0 can be considered as the triplet energy difference the host and guest materials. Based on the above theoretical background, the comparative triplet energies for the host and the guest materials are given in Figure-4. When the values of ΔG^0 approaches 0, corresponding electron transfer rates reach the largest and when the values locate at area far from 0, Dexter energy transfer values will be very slow. Additionally the large free energy change can benefit for the confinement of excitons. $\Delta G^0 >> 0$ means that the confinement of triplet excitons are strongly confined on the host material while $\Delta G^0 << 0$ means that the triplet excitons can be strongly confined on the guest material. For the former case, the investigated system should have long host lifetime to get high EL quantum efficiency. The triplet energies of the studied five guest materials are smaller than those of host materials, namely $\Delta G^0 << 0$, demonstrating that Dexter energy transfer from the host to the guest has taken place. Moreover a maximum efficiency of ~ 13.5 cd/A was achieved for both **1** and **5** with power efficiencies of 5.5 lm/W and 4.7 lm/W at 300 cd/m^2.[22]

If we take the assumption that the dosage concentration is identical for different guest complexes in the device then it can be considered that the distance between the host

and guest can be approximately equal for the different complexes. [refer sec 2.3]. As the host is same for the device, so the transition dipole moment for the donor μ_d is identical for the current matching system. Considering the other factors in the equation to be constant, we can say that $|\langle \Psi_i | V | \Psi_j \rangle|^2$ is solely dependent on the transition dipole moment of the acceptor μ_a, and the calculated values are collected in the Table-4. It shows that the transition dipole moments for the acceptor μ_a are having transition dipole moment in the increasing order as **1**>**2**>**3**>**4**>**5**. In general we can say that if the electron-transporting material used in the device structure is not populated by excitons and provide any appreciable emission the efficient energy transfer from the host to the guest can take place easily.

3.7 Prediction of SOC

Theoretically, the spin orbit coupling is proportional to the distance to the sixth power (according to a qualitative approach for a hydrogen like atom), in which r is the distance between Ir and the ancillary chromophore. In our results, the trend of r is **4>2>1>3>5**. McGlynn et al.[56] suggested that the radiative rate constant k_r could be correlated to the percentage of the metal character (*M* %) in which the spin orbit coupling elements are expected to increase as the content of metal character increases in the corresponding excitation. It is also possible to estimate the amount of metal character in the lowest singlet triplet transition by looking at the product of the squared coefficient of the corresponding TDDFT eigenvector and the percentage of metal character in the starting molecular orbital.[57] With this assumption in mind, we have tabulated the percentage metal character in Table 5. The trend of k_r values could be arranged in the following order **1>3>5>4>2**. It has been demonstrated in the previous studies[58] that the $T_1 \rightarrow T_n$ and $S_0 \rightarrow S_n$ states significantly contribute to S-T transition moment at the optimized geometry and at T_1 state, these contributions will be destroyed. However in our complexes, this contribution is anticipated to be less important as the energy gap values are larger (> 2eV) between these states.[54]

The energy differences between the HOMOs and occupied orbitals with a larger contribution of Ir 5d are one of the important factors to determine the k_r values of

phosphorescence.[59] [refer sec 2.4] In our complexes, the differences in orbital energy between HOMO and HOMO-1 are 0.10 eV for **1**, 0.68 eV for **2**, 0.36 eV for **3** , 0.41eV for **4** and 0.16 eV for **5** reflecting orbital interactions with the ligands. The parentage of the lowest three states is mainly the T_1 state. The lowest states are almost pure triplet state. Spin orbit coupling further restricts the electronic configurations of $^1d\pi^*$, which can be coupled with ^{3} $d\pi^*$ in the lowest triplet state.[59(c)] In our complexes, we have taken the intense phosphorescence of singlet states with highest oscillator strength. Complex **1** originates for the mixing between S_5 and T_1 with oscillator strengths (f_s) 0.0806 in Table 6. It might be possible that the larger contribution of F_2ppy in complex **1** gives rise to the stronger oscillator strength. Similarly the intense phosphorescence comes from S_1 and T_1 with 0.0517, 0.0406, 0.0451 oscillator strength for complexes **2, 4, 5** respectively and S_3 and T_1 with 0.0745 oscillator strength for complex **3**. Using theoretical values of $\zeta_{5d\text{-}Ir}$ =4430 cm^{-1} for the Ir (III) ion, n=1.42 (dichloromethane), eq 9 gives $2.94x10^4$, $3.5x10^4$, $1.43x10^4$, $1.9x10^4$ and $1.6x10^5$ s^{-1} respectively for complex **1, 2, 3, 4** and **5**. These estimated values are also supported by the literature.[59(a,b)] The calculated values are relatively deviated from the experimental values which can be ascribed to the over-simplifications of the spin orbit interactions. So for more reliable evaluation we should consider the spin orbit interactions with many excited states and the geometrical changes of emitting states. Second order perturbation theory can be used to estimate the energetic interactions between the donor lewis-type NBOs and the acceptor non-lewis NBOs. Due to the higher energies of 20.61, 20.59 and 42.10 Kcal/mol for **3**, **4** and **5**, the photo-physical properties of these complexes can be influenced much by these electron-withdrawing groups more than **1** and **2** with 16.13 and 10.77 kcal/mol respectively.

4. Conclusion

This work reports the geometrical structures, absorptions, injection, transport abilities, radiative lifetimes, radiative decay rate k_r, phosphorescence mechanism and the second perturbation energies of five blue-emitting iridium (III) complexes. It has been observed that the substitution pattern has not much influence the absorption. We observe that increasing the electron –withdrawing capabilities leads to a lowering of the HOMO

level with a consequent slight widening of the HOMO-LUMO gap and a blue shift in emission. Introducing the substituents has modulated the emission energy and has changed the ordering of the lowest triplet states. These transitions play major role in defining the radiative decay rate of the complexes. The extent of charge-transfer contributions can also be modified by the HOMO-LUMO gap between the relevant molecular orbitals. Apart from lower S_1-T_1 energy gap (ΔE_{ST}) and larger MLCT contributions, transition dipole moment and percentage metal character may also account for larger k_r values. It can be concluded that by changing the substituents on the triazole fragment we can tune the photophysical properties of the complexes to achieve narrow emission. Our calculations well interpret the matching rules between the host and guest materials for the device structure. Hence, this work can provide guidance for further designing high efficient guest complexes in improving the electroluminescent efficiency. Though, of course, there is still a long way to go for practical applications.

Acknowledgements

One of the author (RS) acknowledges the financial assistance by the DST WOS-A (CS-55/2010). RS is thankful to her Mentor Dr. K. Bhanuprakash, Chief Scientist, CSIR-IICT for useful discussions and calculations.

References

(1) W.Y.Wong, G.J. Zhou, M. Yu, H.S. Kwok, Z.Y. Lin, *Adv. Funct. Mater.* 2007, *17*, 315-323.

(2) W.Y.Wong, C.L. Ho, Z.Q. Gao, B.X. Mi, C.H. Chen, K.W. Cheah, Z.Y. Lin, *Angew.Chem. Int. Ed.* 2006, **45**, 7800-7803.

(3) C.Adachi, M.A. Baldo, S.R. Forest, M.E. Thompson, *Appl. Phys.Lett.* 2000, 904-7.

(4) P.T.Chou, Y .Chi, *Chem. Eur. J.* 2007, **13**, 380-395.

(5) S.R. Forrest, M.E. Thompson, *Chem. Rev.* 2007, **107**, 923-925.

(6) R.C. Evans, P. Douglas, C.J. Winscom, *Coor. Chem. Rev.*, 2006, **250**, 2093-2126.

(7) E. Suljovrujic, A. Ignjatovic, V.I. Srdanov, T. Mitsumori, F. Wudi, *J. Chem. Phys.* 2004, **121**, 3745-3750.

(8) B.Liang, C.Y. Jiang,C. Y, Z. Chen, X.J. Zhang, H.H. Shi, Y. Cao, *J. Mater. Chem.* 2006**, 16**, 1281-1286.

(9) E. Holder, B.M.W.Langeveld, U.S. Schubert, *Adv. Mater.* 2005, **17**, 1109-1121.

(10) P.Coppo, E.A. Plummer, L. De Cola, *Chem. Commun.* 2004, 1774-1775.

(11) Y.You, S.Y. Park, *J. Am. Chem. Soc.* 2005, **127**, 12438-12439.

(12) M.K.Nazeeruddin, R.Hummphry-Baker, D. Berner, S. Rivier, L. Zuppiroli, M. Gratzel, J. *Am. Chem.Soc*. 2003, **125**, 8790-8797.

(13) T. Sajoto, P.I. Djurovich, A. Tamayo, M. Yousufuddin, R. Bau, M.E.Thompson, R.J.Holmes, S.R. Forrest, *Inorg. Chem.* 2005, **44**, 7992-8003.

(14) S.Lamansky, P. Djurovich, D. Murphy, F. Abdel-Razzaq, R. Kwong,I. Tsyba, M. Bortz, B. Mui, R. Bau, M.E. Thompson, *Inorg. Chem.* 2001, **40**, 1704-1711.

(15) I.M. Dixon, J.P. Collin, J.P. Sauvage, L. Flamigni, S. Encinas, F. Barigelletti, *Chem. Soc. Re*v. 2000, **29**, 385-391.

(16) (a) V.V.Grushin, N. Herron, D.D. LeCloux, W.J. Marshall, V.A. Petrovand ,Y. Wang, *Chem. Commun.*, 2001, 1494-1495 (b) K. Dedeian, J.M. Shi, N. Shepherd, E. Forsythe, D.C. Morton, *Inorg. Chem*., 2005, **44**, 4445-4447. (d) Xin Li, Boris Minaev, Hans Ågren, He Tian, *Eur. J. Inorg. Chem.* 2011, 2517–2524.(e) Stefan Kappaun, Christian Slugovc , Emil J. W. List, *Int. J. Mol. Sci.,* 2008, ***9***, 1527-1547

(17) (a) A.B.Tamayo, B.D. Alleyne, P.I. Djurovich, S. Lamansky, I. Tsyba, N.N. Ho, R. Bau, M.E. Thompson, *J. Am. Chem. Soc*., 2003, **125**, 7377-7387. (b) R. Ragni, E.A.

Plummer, K. Brunner, J.W.Hofstraat, F. Babudri, G.M. Farinola, F. Naso, L. De Cola, *J. Mater. Chem.* 2006, **16**, 1161-1170. (c) Huifang Li, Paul Winget, Chad Risko, John S. Sears and Jean-Luc Bre´das, *Phys. Chem. Chem. Phys.,* 2013, **15**, 6293—6302. (d) Xiao-Hong Shang, Yu-Qi Liu, Juan-Juan Su, Godefroid Gahungu, Xiao-Chun Qu, and Zhi-Jian Wu, *International Journal of Quantum Chemistry*, 2014, **114**, 183–191. (e) Yanling Si, Yuqi Liu, Xiaochun Qu, Ying Wang, Zhijian Wu, *Dalton Trans*., 2013, **42**, 14149–14157.

(18) J.Li, P.I. Djurovich, B.D. Alleyne, M. Yousufuddin, N.N.Ho, J.C. Thomas, S.C. Peters, R. Bau, M.E. Thompson, *Inorg. Chem*. 2005, **44**, 1713-1727. (b) I.Avilov, P.Minoofar, J.Cornil, L.De Cola, *J. Am. Chem. Soc*., 2007, **129**, 8247-8258. (c) S.J. Su, H. Sasabe, T. Takeda, J. Kido, *Chem. Mater*., 2008, **20**, 1691-1693 (d) E. Orselli, R.Q. Albuquerque, P.M. Fransen, R. Froehlich, H.M. Janssen, L. De Cola, *J. Mater. Chem*., 2008, **18**, 4579-4590. (e) L.L.Wu, C.H.Yang, I.W. Sun, S.Y. Chu, P.C Kao, H.H. Huang, *Organometallics,* 2007, **26**, 2017-2023.

(19) C.F. Chang, Y.M. Cheng, Y. Chi, Y.C. Chiu, C.C. Lin, G.H. Lee, P.T. Chou, C.C. Chen, C.-H. Chang, C.C. Wu, *Angew. Chem. Int. Ed.* 2008, 47, 4542-4545.

(20) Y.Chi, P.T. Chou, *Chem. Soc. Rev.*, 2010, **39**, 638-655.

(21) Kazuyoshi.Tsuchiya, Shiki.Yagai, Akihide. Kitamura, Takashi. Karatsu, Kyoko. Endo, Junji. Mizukami, Seiji. Akiyama, Masayoshi.Yabe**,** *Eur. J. Inorg. Chem.* 2010, 926–933.

(22) E.Orselli, G.S. Kottas, A.E .Konradsson, P. Coppo, R. Frohlich, L.D. Cola, D.V. Dijken, M. Buchel, H. Borner, *Inorg.Chem* 2007, **46**, 11082-11093. CCDC - 642787 (**3**), 642608 (**4**), 623520 (**5**).

(23) W.R. Browne, R. Hage, J.G. Vos, *Coord. Chem. Rev.* 2006, **250**, 1653-1668.

(24) (a) B.Minaev, V Minaeva , H. Agren, *J. Phys. Chem. A*. 2009, **113**, 726-735. (b) I.Tunnell, Z. Rinkevicius, P. Salek, O. Vahtras, T. Helgaker, H. Agren, J.Chem. *Phys.* 2003, **119**, 11024-11034.

(25) D. Volyniuk, V. Cherpak, P. Stakhira, B. Minaev, G. Baryshnikov, M. Chapran, A. Tomkeviciene, J. Keruckas, J. V. Grazulevicius, *J. Phys. Chem. C* 2013, **117**, 22538.

(26) Boris Minaev, Gleb Baryshnikov, Hans Agren, *Phys. Chem.Chem.Phys.* 2014, **16**, 1719.

(27) T.Guillon, M. Boggio-Pasqua, F. Alary, J.L. Heully, E. Lebon, P. Sutra A. Igau, *Inorg. Chem.* 2010, **49**, 8862-8872.

(28) E. Runge and E. K. U. Gross, Phys. Rev. Lett., 1984, 52, 997-1000.

(29) (a) J. P. Perdew, K. Burke and M. Ernzerhof, Phys. Rev. Lett., 1996, 77,3865-3868. (b) J. P. Perdew, K. Burke and M. Ernzerhof, Phys. Rev. Lett., 1997, 78, 1396.(c) C. Adamo and V. Barone, J. Chem. Phys., 1999, 110, 6158-6169.

(30) (a) R. E. Stratmann, G. E. Scuseria and M. J. Frisch, J. Chem. Phys., 1998, 109, 8218-8224 ; (b) N. N. Matsuzawa, A. Ishitani, D. A. Dixon and T. Uda, J. Phys. Chem. A, 2001, 105, 4953-4962. (c) M. E. Casida, C. Jamorski, K. C. Casida and D. R. Salahub, J. Chem. Phys., 1998, 108, 4439-4449.

(31) M. Cossi, G. Scalmani, N. Regar and V. Barone, J. Chem. Phys., 2002, 117, 43-54.

(32) V. Barone, M. Cossi and J. Tomasi, J. Chem. Phys., 1997, 107, 3210-3221.

(33) P.J. Hay, *J. Phys. Chem. A* 2002, **106,** 1634-1641.

(34) M. J. Frisch, G. W. Trucks, H. B. Schlegel, G.E. Scuseria, M.A. Robb, J.R. Cheeseman, J. A. Jr. Montgomery, T. Vreven, K.N. Kudin, J.C. Burant, J.M. Millam, S.S. Iyengar, J. Tomasi, V. Barone, B. Mennucci, M. Cossi, G. Scalmani, N. Rega, G.A. Petersson, H. Nakatsuji, M. Hada, M. Ehara, K. Toyota, R. Fukuda, J. Hasegawa, M. Ishida, T. Nakajima, Y. Honda, O. Kitao, H. Nakai, M. Klene, X. Li, J.E. Knox, H.P. Hratchian, J.B. Cross, C. Adamo, J. Jaramillo, R. Gomperts, R.E. Stratmann, O. Yazyev, A.J. Austin, R. Cammi, C. Pomelli, W. J. Ochterski, P.Y. Ayala, K. Morokuma, G.A. Voth, P. Salvador, J.J. Dannenberg, V.G. Zakrzewski, S. Dapprich, A.D. Daniels, M.C. Strain, O. Farkas, K. D. Malick, D.A. Rabuck, K.Raghavachari, J.B. Foresman, J.V. Ortiz, Q. Cui, A.G. Baboul, S. Clifford, J. Cioslowski, B.B. Stefanov, G.Liu, A. Liashenko, P. Piskorz, I. Komaromi, R.L. Martin, D.J. Fox, T. Keith, M.A. Al-Laham, C.Y. Peng, A. Nanayakkara, M. Hallacombe, CP.M.W. Gill, B. Johnson, W. Chen, M.W. Wong, C. Gonzalez, J.A. Pople, J. A.C.02; Gaussian, Inc.: Wallingford, CT, 2009.

(35) N.M.O.Boyle, A.L. Tenderholt, K.M. Langner, *J. Comput. Chem.* 2008, ***29***, 839-845.

(36) F. Weinhold, C.R. Landis, Chem Ed. Res. Practice Eur. 2001, **2**, 91-104.

(37) Oskar Rubio-Pons, Oleksandr Lobada, Boris Minaev, Bernd Schimmelpfennig, Olav. Vahtras and Hans Agren, *Mol. Phys.* 2003, **101**, 2103-2114.

(38) N.S.Hush, *J. Chem. Phys.* 1958, **28**, 962-972.

(39) R.A. Marcus, J. *Chem. Phys.* 1956, **24**, 966-978.

(40) (a) M. Malagoli, J.L. Bredas, *Chem. Phys. Lett.* 2000, **327**, 13-17.(b) B.C. Lin, C.P. Cheng, Z. Ping, M.J. Lao, *Phys. Chem. A* 2003**, 107**, 5241-5251. (c) K. Sakanoue, M. Motoda, M. Sugimoto, S. Sakaki, *J. Phys. Chem. A* 1999, **103**, 5551-5556. (d) Y.Z.Lee, X.W. Chen, S.A. Chen, P.K. Wei, W.S. Fann, *J. Am. Chem. Soc.* 2001, **123**, 2296-2307.

(41) G. R. Hutchison, M. A. Ratner, T. J. Marks, *J. Am. Chem. Soc.* 2005, **127**, 2339-2350.

(42) (a) S.H. Lin, W.Z. Xiao and W. Dietz, *Physical Review E*, 1993, **47**, 3698-3706. (b) J. Han, X. Chen, L. Shen, Y. Chen, W. Fang and H. Wang, *Chem. Eur. J.*, 2011, **17**, 13971-13977.

(43) Z. Abedin Siddique, Y. Yamamoto, T. Ohno, K. Nozaki, Inorg. *Chem*. 2003, **42**, 6366-6378.

(44) S. Hander, E.D. Como, J. Feldmann, J.M. Lupton C. Lennartz, P. Erk, E. Fuchs, O. Molt, I. Munster, C. Schildknecht, G. Wagenblast, *Adv. Mater*. 2008, **20**, 3325-3330.

(45) T.Azumi, H. Miki, *Top. Curr. Chem.*1997, **191**, 1.

(46) E.A. Solomon, A.B.P. Lever, *Inorganic Electronic Structure and Spectroscopy*, Vol.I, Chapter 1; Wiley: New York, 1999, **1**, Chapter 10, 555.

(47) K. Nozaki, *J. Chin. Chem. Soc.* 2006, **53**, 101-112.

(48) S.Fraga, K.M.S. Saxena, J. Karwowski, Handbook of Atomic Data Physical Sciences Data, Vol.5; Elsevier: Amsterdam, The Netherlands, 1976.

(49) C.S.K. Mak, A. Hayer, S.I. Pascu, S.E. Watkins, A.B. Holmes, A. Kohler, R.H. Friend, *Chem. Commun.* 2005, **37**, 4708-4710.

(50) Asanga B Padmaperuma, *Molecular Simulation*, 2013, **39**, 405–414.

(51) Lei-Jiao. Li, Ji-Kang. Feng , Ai-Min. Ren, *J. Phys. Org. Chem*. 2009, ***22***, 118-124.

(52) Xiao-Na. Li, Zhi-Jian. Wu, Si Zhen-Jun , Hong-Jie, Zhang, Zhou Liang, *Inorganic Chemistry ,* 2009, **48**, 7740-7749.

(53) S. C. Lo, C. P. Shipley, R. N. Bera, R. E. Harding, A. R. Cowley, P. L. Burn, I.D.W. Samuel, *Chem. Mater.* 2006, **18**, 5119-5129.

(54) (a) X. N. Li, X. J. Liu, Z. J. Wu, H. J. Zhang *J. Phys. Chem. A* 2008, **112**, 11190-11197. (b) X. N. Li, J.K. Feng, A.M. Ren, Chin. *J. Chem*. 2008, **26**, 1979-1984. (c) Y.L. Liu, J.K. Feng, A.M. Ren, *J. Phys. Org. Chem.* 2007, **20** ,600-609.

(55) Youtian Tao, Chuluo Yang and Jingui Qin, *Chem. Soc. Rev.,* 2011, **40,** 2943-2970.

(56) S.P. McGlynn, T. Azumi, M. Kinoshita, Molecular spectroscopy of triplet state; Prentice Hall: Englewood Cliffs, NJ, 1969, p 434.

(57) Xin Li, Qiong Zhang, Yaoquan Tu, Hans Ågren and He Tian, *Phys. Chem. Chem. Phys.,* 2010, **12**, 13730-13736.

(58) Xin Li, Boris Minaev, Hans Ågren and He Tian, *J. Phys. Chem. C,* 2011, **115**, 20724–20731.

(59) (a) J. Wang, F-Q. Bai,B.H. Xia, H.X. Zhang, *J. Phys. Chem.* 2011, **115**, 11689-11695.(b) Qi. Cao, Zai-Feng. Xie, Jing. Wang, Zhao-Shuo. Tian. Fu-Quan. Bai, *Molecular Physics***,** 2012, **110**, 185-197. (c) Q. Cao, J. Wang, Z.S. Tian, Z.F. Xie, F.Q. Bai, *J. Comput. Chem.,* 2012, **33**, 1038-1046.

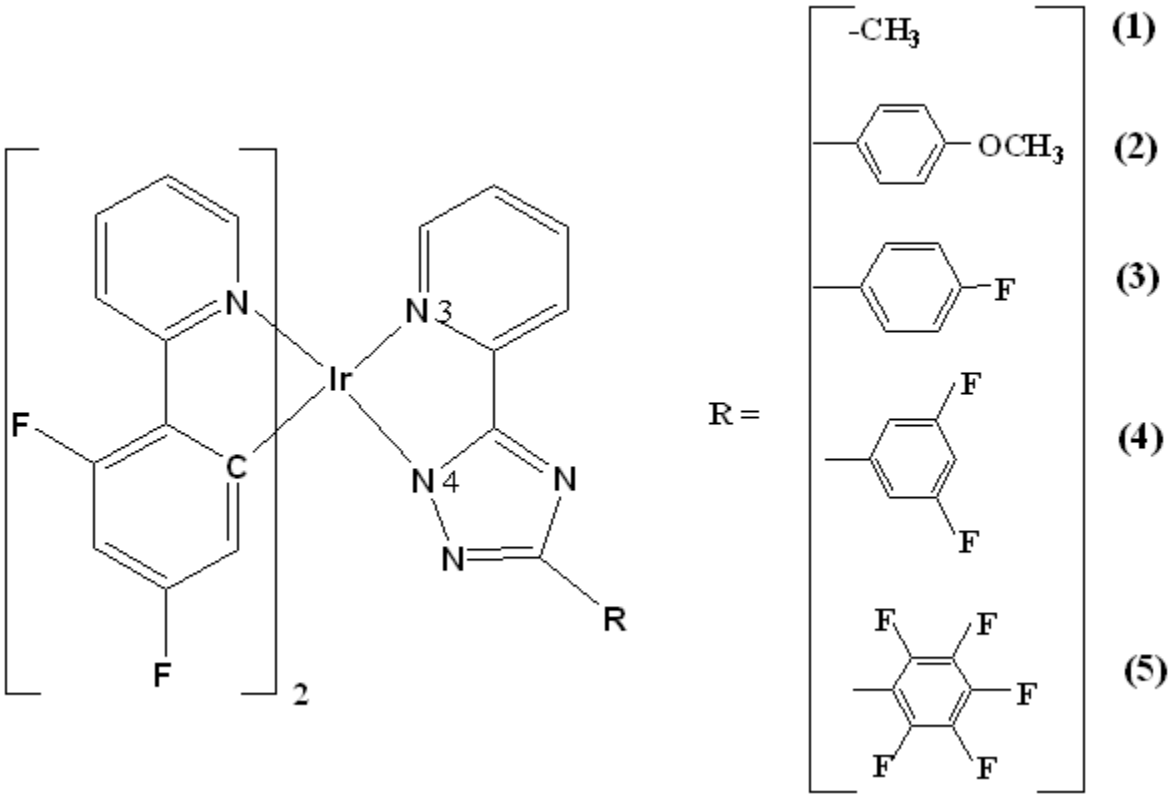

Figure 1: Sketch structures of the complexes (1-5).

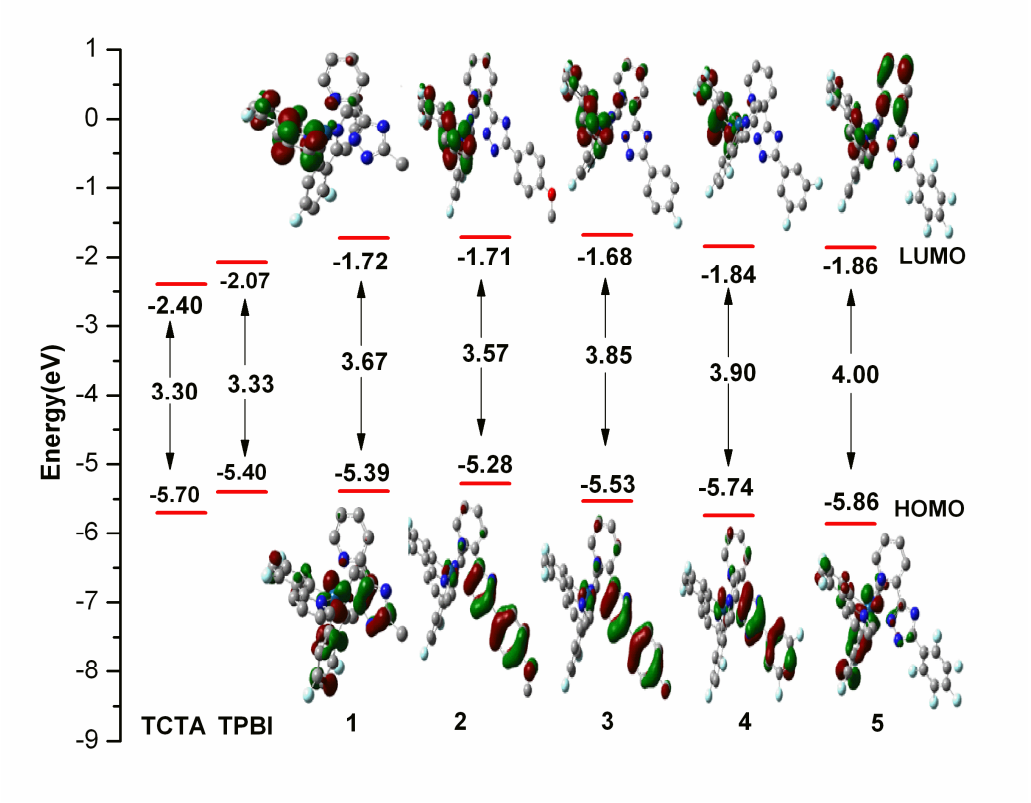

Figure 2: Presentation of the energy levels, HOMO-LUMO gap and orbital composition distribution of the HOMO and LUMO for (1-5) complexes. The energy levels, HOMO-LUMO gap for host material[22] (TCTA, TPBI) are also given for comparison.

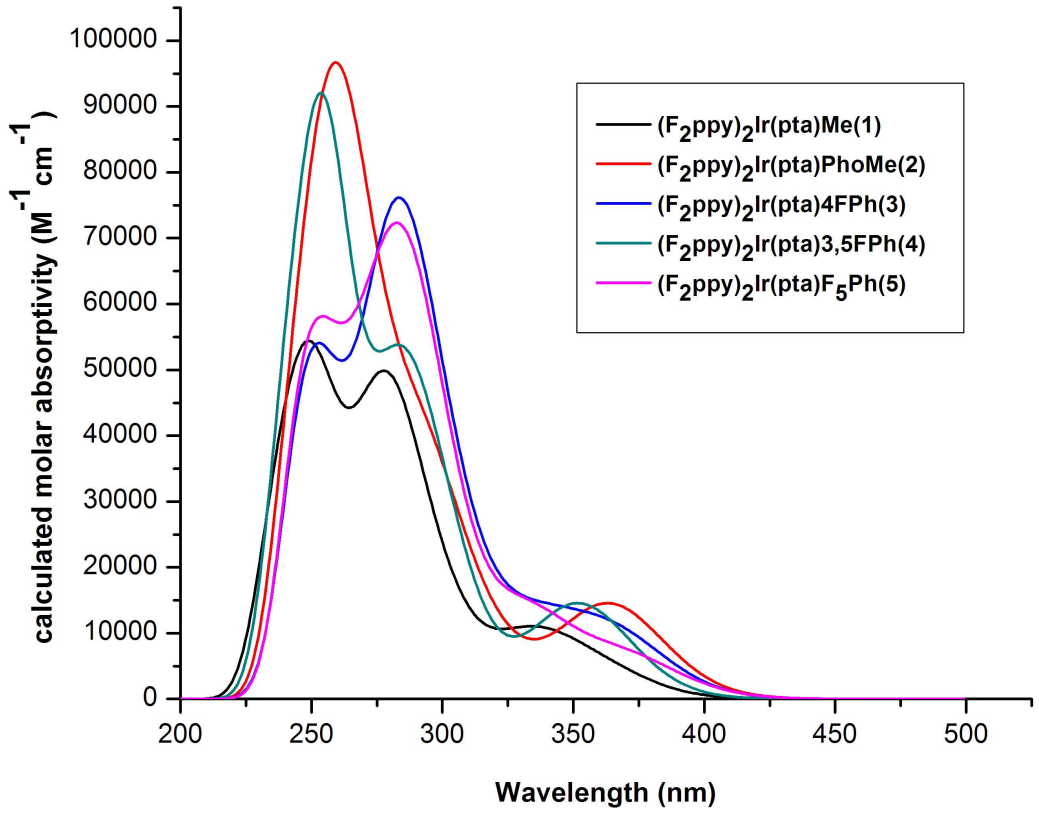

Figure 3: Calculated Absorption spectra for (1-5) in dichloromethane.

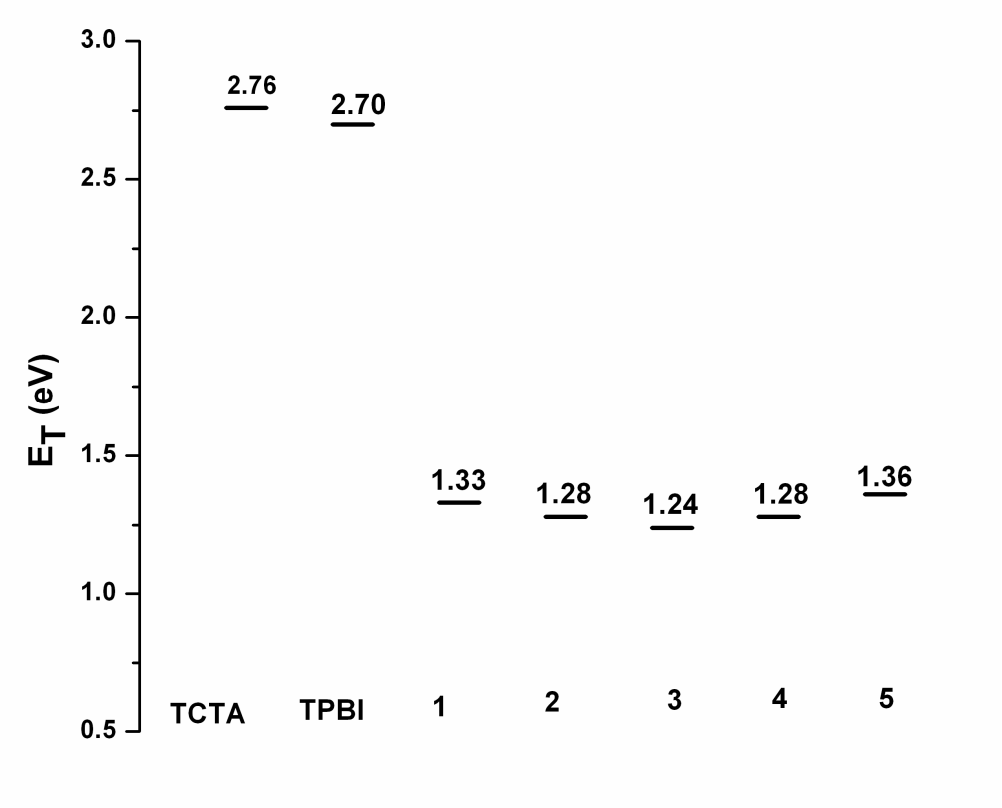

Figure 4: Triplet energies of the host (TCTA, TPBI) and studied guest materials (1-5). [The triplet energies for the host materials are taken from ref. 22]

Table 1 . Main Optimized Geometry Structural Parameters of (1-5) in the Ground and the Lowest Lying Triplet States.

	Bond-Length (Å)									
Complexes	**1**		**2**		**3**		**4**		**5**	
	S_0	**T_1**	**S_0**	**T_1**	**S_0**	**T_1**	**S_0**	**T_1**	**S_0**	**T_1**
Ir-N1	2.047	2.047	2.048	2.049	2.045	2.048	2.047	2.047	2.045	2.033
Ir-N2	2.045	2.048	2.046	2.046	2.059	2.049	2.047	2.049	2.058	2.056
Ir-C1	1.996	2.011	2.008	2.005	1.988	2.004	2.008	2.010	1.978	1.998
Ir-C2	2.009	2.004	1.996	2.009	2.011	2.010	1.997	2.005	2.008	1.986
Ir-N3	2.203	2.088	2.116	2.090	2.083	2.089	2.119	2.171	2.234	2.203
Ir-N4	2.117	2.171	2.202	2.169	2.226	2.171	2.204	2.089	2.085	2.080
	Bond-Angle (deg)									
N3-Ir-N4	75.9	77.3	75.9	77.8	75.9	77.3	75.9	77.3	75.9	76.6
N3-Ir-C2	95.2	96.6	96.6	97.2	98.2	97.2	98.2	97.1	98.3	97.4
	Dihedral Angle (deg)									
N1-N2-Ir-N3	154.4	155.9	129.9	129.3	130.3	131.3	131.9	131.5	139.9	139.5
C1-N3-Ir-C2	153.9	153.6	153.6	154.7	155.6	155.6	155.0	155.9	155.6	155.1

Table 2: Excitation energy, oscillator strength, configuration interaction (*CI*) Coefficient and major electronic configuration for the complexes along with experimental wavelengths.

	λ(nm) cal	*E*(eV) cal	*f*	CI Coeff.	Configurations	λ(nm) expt.	Assignments
Complex 1							
S_1	363	3.42	0.0491	0.6643	H→L(83%)	374	MLCT/LLCT
S_2	353	3.51	0.0069	0.6227	H→L+1(80%)		MLCT/ILCT
S_3	346	3.59	0.0419	0.5805	H→L+2(71%)		MLCT/LLCT
S_4	342	3.62	0.0176	0.6610	H-1→L(72%)		MLCT/LLCT
S_5	334	3.71	0.0806	0.5746	H-1→L+1(56%)	343	MLCT/LLCT
S_6	325	3.81	0.0376	0.5863	H-1→L+2 (69%)		MLCT
S_7	303	4.09	0.0229	0.6643	H→L+3 (88%)		MLCT/LLCT
S_8	302	4.10	0.0822	0.4610	H-2→L(43%)		MLCT/LLCT
S_9	299	4.15	0.0237	0.3843	H-2→L+1 (30%)		MLCT/LLCT
S_{10}	294	4.22	0.0158	0.4555	H-1→L+3 (41%)	282	MLCT/LLCT
T_1		1.33		0.2347	H-1→L(67%)		
Complex 2							
S_1	373	3.32	0.0517	0.6443	H→L(88%)		MLCT/LLCT
S_2	367	3.38	0.0895	0.6325	H→L+1(78%)	370	MLCT/LLCT
S_3	363	3.42	0.0085	0.5949	H→L+2(67%)		MLCT/ILCT
S_4	358	3.46	0.0549	0.5992	H-1→L(87%)	354	MLCT/LLCT
S_5	346	3.58	0.0202	0.5280	H-1→L+1(66%)		MLCT/LLCT
S_6	343	3.62	0.0154	0.5158	H-1→L+2 (53%)		MLCT/LLCT
S_7	319	3.89	0.0927	0.6800	H→L+3 (92%)		LLCT
S_8	303	4.09	0.0818	0.3840	H→L+4 (29%)		MLCT/LLCT
S_9	302	4.10	0.0269	0.5133	H→L+4 (53%)		MLCT/LLCT
S_{10}	301	4.11	0.0286	0.5271	H-1→L+3 (56%)		MLCT/LLCT
T_1		1.28		0.4123	H→L+4(61%)		
Complex 3							
S_1	375	3.31	0.0329	0.6145	H→L(76%)	370	MLCT/LLCT
S_2	367	3.37	0.0243	0.4988	H→L+2(50%)		MLCT/ILCT
S_3	365	3.40	0.0745	0.5188	H→L+1(54%)		MLCT/ILCT

S_4	347	3.57	0.0294	0.6165	H-1→L(76%)		MLCT/LLCT
S_5	338	3.67	0.0895	0.6627	H-1→L+1(76%)	342	MLCT/ILCT
S_6	333	3.72	0.0293	0.6462	H-1→L+2 (84%)		MLCT/LLCT
S_7	318	3.90	0.0865	0.6824	H→L+3 (93%)	315	MLCT/ILCT
S_8	302	4.10	0.2217	0.3661	H-1→L+3 (27%)		LLCT/ILCT
S_9	301	4.11	0.0064	0.5580	H→L+4 (62%)		MLCT/LLCT
S_{10}	300	4.12	0.0375	0.3742	H→L+5 (28%)		MLCT/ILCT
T_1		1.24		0.7748	H→L+2(60%)		
Complex 4							
S_1	363	3.42	0.0406	0.4812	H-1→L(46%)	370	MLCT/LLCT
S_2	356	3.49	0.1007	0.5063	H→L+1(51%)		MLCT/LLCT
S_3	354	3.51	0.0061	0.4708	H→L+2(44%)		MLCT/ILCT
S_4	350	3.54	0.0188	0.4168	H-1→L(35%)		LLCT/ILCT
S_5	343	3.61	0.0416	0.5981	H-1→L+1(72%)	346	MLCT/LLCT
S_6	336	3.68	0.0344	0.4978	H-1→L+2 (50%)		MLCT/LLCT
S_7	307	4.03	0.065	0.6372	H→L+3 (81%)	315	MLCT/ILCT
S_8	302	4.10	0.1216	0.4198	H-2→L (35%)		MLCT/ILCT
S_9	300	4.13	0.0126	0.5708	H-1→L+3 (65%)		LLCT/ILCT
S_{10}	298	4.16	0.0179	0.4237	H-2→L+2 (36%)		LLCT/ILCT
T_1		1.28		0.5057	H→L+2(26%)		
Complex 5							
S_1	377	3.29	0.0451	0.6432	H→L(83%)	370	MLCT/ILCT
S_2	367	3.38	0.008	0.6313	H→L+2(80%)		LLCT/ILCT
S_3	364	3.41	0.0463	0.6308	H→L+1(80%)		LLCT/ILCT
S_4	341	3.63	0.0178	0.6407	H-1→L(82%)	350	MLCT/ILCT
S_5	334	3.71	0.1294	0.6750	H-1→L+1(91%)		MLCT/LLCT
S_6	327	3.79	0.0275	0.6738	H-1→L+2 (91%)		MLCT/LLCT
S_7	317	3.91	0.0434	0.6747	H→L+3 (91%)		MLCT/ILCT
S_8	302	4.11	0.0635	0.3334	H-2→L (22%)		MLCT/LLCT
S_9	301	4.12	0.1442	0.4571	H-2→L (22%),		MLCT/LLCT
S_{10}	300	4.15	0.0748	0.4462	H→L+5 (40%)		MLCT/ILCT
T_1		1.36		0.7000	H→L+2(49%)		

Table 3: Calculated Emission and radiative lifetimes (τ) for (1-5).

Complex	E (eV)	λ_e (nm)	f	τ(μs)	Main Configurations	λ_e (nm) (exp)
1	2.90	428	0.030	0.09	HOMO→LUMO (96%)	461
2	2.40	517	0.001	3.34	HOMO→LUMO (96%)	492
3	2.75	450	0.017	0.18	HOMO→LUMO (85%)	459
4	2.93	423	0.018	0.15	HOMO→LUMO (64%)	459
5	2.92	425	0.018	0.15	HOMO→LUMO (83%)	458

Table 4: IP, EA, Extraction potentials, reorganization energies, small polaron energies in (eV) and transition dipole moment (ground state) in (D) for (1-5).

Complex	IP_V	IPa	EA_V	EAa	HEP	EEP	λ_h	λe	SPE(h)	SPE(e)	μ_a (D)
1	6.49	6.37	0.42	0.50	6.35	0.59	0.14	0.17	0.12	0.08	1.77
2	6.34	6.16	0.50	0.57	6.16	0.65	0.18	0.15	0.18	0.07	2.09
3	6.69	6.59	0.64	0.72	6.45	0.83	0.24	0.19	0.10	0.08	2.98
4	6.76	6.69	0.64	0.73	6.53	0.84	0.23	0.20	0.07	0.09	2.77
5	6.91	6.78	0.66	0.73	6.56	0.94	0.35	0.28	0.13	0.07	3.03

Table 5: Calculated metal character of phospherescence for (1-5) alongwith the calculated radiative deactivation rate constant with configuration interaction (CI) coefficient of lowest energy singlet-triplet transition at the T_1 geometry

Complex	CI Coeff	Ir character (%)	k_r/s^{-1}
1	0.9824	84.47	$2.9x10^4$
2	0.9826	10.61	$3.5x10^4$
3	0.9844	37.00	$1.4x10^4$
4	0.9843	18.28	$1.9x10^4$
5	0.8957	21.35	$1.6x10^5$

Table 6: Data used for the measurement of phosphorescence radiative rate constants and the evaluation of spin-orbital coupling (SOC) value

Complex	**1**	**2**	**3**	**4**	**5**
	T_1	T_1	T_1	T_1	T_1
E/ev[a]	1.33	1.28	1.24	1.28	1.36
C_{dxy}[b]	0.80	0.79	0.82	0.79	0.77
	S_5	S_1	S_3	S_1	S_1
E/ev[a]	3.71	3.32	3.4	3.42	3.29
C_{dyz}[b]	0.77	0.76	0.79	0.78	0.74
f[a]	0.0806	0.0517	0.0745	0.0406	0.0451
SOC(S_1-T_1)cm^{-1}	1347	1400	1434	1365	947
k_r/s^{-1}(cal)[d]	2.94×10^4	3.5×10^4	1.43×10^4	1.9×10^4	1.6×10^5
k_r/s^{-1}(exp)$\times10^5$	3.9	1.2	2.9	2.1	3.0
n=1.42					

[a] Obtained from the calculation. [b] Coefficient of the natural atomic orbital of Ir 5d in the HOMO (T_1) or HOMO -1 (S_1) obtained from NBO analysis. [c] Absolute value of the spin-orbit coupling matrix element calculated from eq. (10). [d] Value calculated via the eq. (9).